Optimization of blade curvature and inter-rotor spacing of Savonius rotors for maximum wave energy extraction

M. Rafiuddin Ahmed[1*], Mohammed Faizal[2] and Young-Ho Lee[2]

1. The University of the South Pacific, Laucala Campus, Suva, Fiji
2. Korea Maritime University, 1 Dongsam-dong Youngdo-ku, Busan, South Korea
Email: ahmed_r@usp.ac.fj

ABSTRACT

The water particles are known to undergo orbital motion in wave motion. This orbital motion was studied and seven Savonius rotors with same diameters but different blade angles were constructed and tested in a wave channel to find the optimum blade angle. Experiments were carried out in a two-dimensional wave channel on intermediate depth waves. The submergence of the rotors below the mean water level was varied. The optimum blade curvature for maximum energy extraction was found to be 70^o from the rpm measurements. Two arrays of rotors with this blade curvature were then employed at different depths to study the energy extraction from the orbital motion. The flow around the rotors was documented with particle image velocimetry (PIV) measurements. It was found that the optimum performance of the rotors is obtained at the minimum spacing between the rotors. Experiments carried out with two arrays showed that the maximum energy extraction from the orbiting particles takes place when the gap between the upper and lower arrays is less. This concept can be extended to multiple arrays with reducing rotor diameters at deeper submergences.

Key words: wave energy; orbital motion; Savonius rotor, particle image velocimetry.

Nomenclature

a wave amplitude, m

d outer diameter of Savonius rotor, m

D mean water depth, m

f wave frequency, Hz

H wave height, m

k wave number, m^{-1}

N_n non-dimensioned rotor rpm

x streamwise coordinate, m

y transverse coordinate, m

z vertical coordinate, m

λ wavelength, m

θ phase position, degrees

1. Introduction

The water waves propagate on the ocean surface as a result of a generating force (Dalrymple and Dean, 1991) and the most common generating force is the energy transfer from wind to water by the frictional drag of the air on the ocean surface (Janssen, 2004). Ocean waves are always present as long as there is wind blowing over the ocean surface, thus offering a continuous source of wave energy (Janssen, 2004). The power flow in the waves is about five times compared to the wind that generates the waves, making wave energy more persistent than wind energy (Falnes, 2007). Wave energy is attracting a lot of attention now, as it is available 90% of the time at a given site compared to solar and wind energies which are available 20 - 30% of the time (Pelc and Fujita, 2002).

Water waves can be classified into two categories: oscillatory waves and translatory waves. In oscillatory waves, the average mass transport of water is zero. It is only the wave form that moves through the water, and the motion of the waves sets the water particles in orbital motion (Pickard and Pond, 2000). Translatory waves involve the mass transport of water in the direction in which the waves travel (Mehaute, 1976). Examples of translatory waves are waves formed by floods in rivers and tidal bores. Waves are easily studied by assuming it to be regular sinusoids with common characteristics of wave period, wavelength, and wave height (Dalrymple and Dean, 1991; Pickard and Pond, 2000). Due to the complexity and irregularity of wave motions on the ocean surface, idealized solutions are normally considered for mathematical analysis. It is convenient to study two-dimensional waves generated in tanks with parallel side-walls. Boundary layer effects can be neglected, as they are very small (Mehaute, 1976). The study of velocity distributions and particle flow under waves is essential for design of ocean structures. Particle image velocimetry (PIV) is an optical, non-intrusive, method of velocity measurement that is able to measure particle velocities over a large two dimensional area of a flow field. The flow is seeded with particles, which are illuminated and their positions recorded photographically (Stagonas and Muller, 2007). The water particles for both deep water waves ($D>\lambda/2$, where λ is the wavelength) and shallow water waves ($D<\lambda/20$) undergo orbital motion. In deep water the particle motion is circular and the wave action decreases with depth, but in shallow water the orbits are elliptical and the effect of waves is felt up to the bottom. The motions of the particles are shown in Fig. 1. The radius of the circular orbits in deep water decreases with increasing depth and ceases at $z < -\lambda/2$. In shallow water, the length of the minor axis decreases with increasing depth while that of the major axis remains constant till the bottom; which means the effect of waves is felt till the bottom (Falnes, 2007; Holthuijsen, 2007). Waves that fall in between shallow and deep water waves are termed as intermediate depth waves. Mathematical analysis is mostly done for shallow and deep water waves, since equations do not simplify for intermediate depth waves (Rahman, 1994).

The total energy in a wave is proportional to the square of its height and is equally divided between the kinetic and potential energies: kinetic energy of the water particles motion and gravitational potential energy associated with vertical position of water from the mean level. A higher wave has larger kinetic and potential energies (Falnes, 2007; Pedlosky, 2003). The maximum energy of the

water particles orbital motion is available closer to the free ocean surface (Chang et al., 2007).

Wave energy can be extracted by using a number of systems (Falnes, 2007; Mehaute, 1976; Twidell and Weir, 2006). The kinetic energy of the water particles in orbital motion can be used to drive small Savonius rotors (Jobb, 2008) or water wheels (Mehaute, 1976). Particle motion-based energy extraction devices obtain energy from the moving water particles. The moving elements of the energy extraction device should have their motions matching those of the orbiting water particles (McCormick, 2007). Faizal et al. (2010) utilized the orbital motion in water waves to drive a five bladed Savonius rotor. They presented the performance of this rotor against various wave parameters. It has been found that the rotor performs best when placed closest to the surface, where the maximum wave energy is available. S. J. Savonius had obtained power outputs by using rotors with its axis horizontal and perpendicular to the direction of wave propagation (Merriam, 1978). Recently, Hindasageri et al. (2011) experimentally studied the effect of number of blades and submergence on the rotational speeds of a Savonius rotor. In another work, Hindasageri et al. (2012) studied the effect of wave height and ocean depth on the performance of a Savonius rotor. They found that rotors with five blades performed better when submerged fully. They also found that the wave height and the time period both influence the rotor speed and power output.

Savonius rotor spins due to the differential drag on the curved surfaces (Twidell and Weir, 2006). These rotors develop high torque at low rotational speeds, but have a low power coefficient (Reupke amd Probert, 1991). Effective rotation of the rotor depends on the wave height which also determines the size of the orbits in all types of water waves (Holthuijsen, 2007; Rahman, 1994). The diameter of the rotors should be less than the length of the rotor and the wave height (Jobb, 2008; Faizal et al. 2010). The longer rotor gives more contact area between the blades and water, hence more momentum. Due to the orbital motion, there will always be a strong component of flow striking the concave surface of the blades (angular momentum transfer). A number of rotors can be parallelly mounted in an array with their axis horizontal and normal to the direction of wave propagation. The ends of each rotor will have small dynamos to convert the mechanical energy of the rotors to electrical energy. There can be multiple arrays of Savonius rotors in a given area of the ocean (Jobb, 2008; Ahmed et al., 2010).

The present work is a continuation of the work reported by Faizal et al. (2010) and Ahmed et al. (2010). Five bladed Savonius rotors with different blade curvatures were experimented to find out which geometry gives optimum N_n (non-dimensional rpm) values and then two arrays of the best geometry rotors were tested for maximum energy extraction at different spacings and submergences of the rotors.

2. Experimental Method

The experiments were carried out in a Cussons Wave Channel, model P6325, available in the Thermo-fluids Laboratory of the University of the South Pacific. The wave channel has a length of 3500 mm, a width of 300 mm and a depth of 450 mm. The sidewalls are made of Plexiglas to allow a clear view of the wave action. A flap type wave-maker, hinged at the bottom, produces sinusoidal waves with characteristics of deep water waves (Rea, 2008). The wave-maker is made up of two parts – the mechanical wave generator consisting of the framework, motor and flap, and the electrical control box. By adjusting the frequency of the wave-maker control, waves with different parameters can be generated. A frequency range of 0–1.4 Hz can be set. The frequency set at the wave-maker digital display is equal to the frequency of the waves and was verified by measuring the period and taking its reciprocal; the maximum difference is ±2%. The close fit of the wave-maker to the channel sides ensures that two-dimensional waves are produced with no fluid motion normal to the sidewalls (Rea, 2008). Figure 2 shows a schematic diagram of the wave channel.

The wave height and the wavelength at a given depth are decided by the wave frequency and cannot be controlled independently. The water flow is generated by a centrifugal pump having a rated capacity of 40 L/s at a total head of 10 m and driven by a 5.5 kW motor. The pump draws water from a tank of 1.5 m x 0.8 m cross section which receives back the discharged water from the wave channel. To minimize wave reflection, a Cussons tuneable Beach, model P6285, was installed at the end of the wave channel. It employs a series of porous plates with different porosity levels and variable spacing to absorb the wave energy gradually.

The rotors that were initially tested for optimum geometry have a length of 300 mm and an outer diameter (d) of 66 mm, which is based on the diameter of the orbits close to the surface at the frequency of 0.9 Hz. For a water depth of 260 mm, the diameter of orbits at a depth of about 25 mm for a frequency of 0.9 Hz is obtained using the equation:

$$r = ae^{kz}$$

The wavelength is about 0.7 m and the wave amplitude is 0.041 m (Faizal et al. 2011).

The rotors have five blades each which are made of Aluminum sheets bent at 60º, 65º, 70º, 76º, 80º, 85º, and 90º. Roller bearings were mounted at the shaft ends for friction-free rotation. The shaft diameter is 6 mm. The rotors were placed across the width of the wave channel and parallel to the wave front. The geometric details of the Savonius rotors are shown in Fig. 3.

The wave height and the wavelength were measured using Seiki pressure transducers, model PSHF002KAAG. The data were acquired on a GL500A midi-LOGGER dual data logger, which was connected to the pressure transducers. The wave period was measured by recording the time taken for two successive crests to pass a given point. The water depth was kept constant at 260 mm and the wave frequency was kept constant at 0.9 Hz for this round of experiments. The ratio of mean water depth (D) to the wavelength (λ) was slightly less than 0.4 in the present sets of experiments, indicating that the water particles were not following perfectly circular orbits, but elliptic orbits (intermediate depth) with the major axis only slightly larger than the minor axis. A comparison of the experimental wave characteristics in the present wave channel with the theoretical characteristics is presented by Faizal et al. (2011).

The rotors were tested at submergences of *1.06d*, *1.36d*, and *1.67d*. The distance of the rotors from the wave-maker paddle was more than twice the depth of the hinge to ensure that fully developed waves are formed (Rea, 2008). The rpm of the rotors were recorded with a Compact Instruments optical tachometer, model CT6LSR. The tachometer has an accuracy of 0.01% and a resolution of $\pm$1 rpm.

PIV measurements were performed to study the flow around the rotors. Poly vinyl chloride tracer particles, with an average diameter of 100 μm and specific gravity of 1.02, were seeded into the water. Two 500 mW air-cooled diode-pumped solid state continuous light lasers with an output of 532 nm were employed to obtain a laser sheet and illuminate the particles. The motion of the particles was captured by a high-speed Photron CCD camera. The camera recorded 125 frames per second, producing up to 1280 × 1024 pixel images. The images captured by the CCD camera were processed using Cactus 3.3 software.

In the second round of experiments, the diameter of the rotor was increased and it was found that a diameter of 86 mm gives higher energy extraction from the waves when placed close to the water surface for the mean water depth of 290 mm. Most of the testing was done at the wave frequencies of 0.9 Hz and 1.0 Hz. The final round of experiments was carried out with the two rotor diameters of 86 mm and 66 mm with the larger diameter rotors forming the upper array and the smaller diameter rotors forming the lower array. Table 1 shows the experimental variables and the settings in the present work. Only a few selected results are presented here.

The maximum error in the measurements of rpm of the rotors was recorded at lower rotational speeds when the rotor was ‘slipping’ a little and hence the tachometer was giving erroneous measurements; the maximum error was estimated by comparing the physically observed rpm with the tachometer rpm and was found to be 3.33%; however, as only the non-dimensional rpm values are reported in the present paper, the error will be much less. The factors which were considered for determining the accuracy of velocity measurements with PIV are: the uncertainties due to finite time sampling, finite displacement of the particles, and uncertainties in measuring the displacements of the particle images (Raffel et al. 1998). The accuracy of displacement measurements with Cactus is of the order of 0.1 pixel. For the high-speed camera, the time resolution for the current measurements was 0.008s. To get an accurate estimate of the error in our measurements, most of which were for rotating (orbital) motion of particles, PIV measurements were performed on a calibrated, constant speed rotating motion and the maximum error was found to be 0.32%.

3. Results and Discussion

The results are presented and discussed in this section. A total of seven rotors were studied by recording their rpm. The rotor rpm is non-dimensionalized with the minimum rpm, which was for the 60º rotor at a submergence of *1.67d*. It was observed that the rotor with 90º curvature did not have a full rotation, even at higher frequencies. Figure 4 shows the variations of the rotor rpm with different blade curvatures, for a wave generator frequency of 0.9 Hz and different submergence levels (rotor submergences of *1.06d*, *1.36d* and *1.67d*). It can be seen that the non-dimensional rpm, N_n , peaks for a blade curvature of 70º for all submergences. The rotational speeds of the rotors decrease with increasing submergence (greater depths) because the size of the particle orbits decrease, thus transferring less energy to the blades of the rotors. The maximum energy of the water particles in orbital motion is available closer to the surface (Chang et al., 2007). Also, the translational energy is maximum at the surface. For a submergence of 50 mm, Hindasageri et al. (2011) reported that a 5-bladed rotor has the highest rotational speed. They subsequently proposed a term frequency ratio (*N/f*) to non-dimensionalize the rpm (Hindasageri et al. 2012).

Detailed PIV measurements were performed for a number of rotors and rotor combinations to study the flow characteristics around them. Figure 5 shows the velocity vectors around the 76º rotor for the phase position of $\theta = 0^o - 90^o$ (the particles rising and moving with the crest, where $\theta = 0^o$ corresponds to the crest) at a frequency of 0.9 Hz and the submergence of *z/d = -1.06*. The orbital motion of the particles formed by the crest and trough drives the rotor. The curved blades of the rotor are properly aligned to receive the energy of the orbiting particles and the direction of rotation of the rotor matches the orbital motion. When the crest approaches, there is a strong velocity component in the x-direction on top of the rotor which imparts considerable momentum to the blades that receive that flow. As seen in Fig. 5, the particles rise and move forward with the crest, transferring a significant portion of their kinetic energy to the blades located in the front part of the rotor at that instant. When the particles fall and move backwards with the trough (phase position θ = 180º - 270º, not shown), they transfer a significant portion of their kinetic energy to the blades on the rear side.

The momentum imparted to the blades on the curved surfaces by the orbiting particles causes the rotation. The curved blades are aligned so that there is always a directional flow striking the concaved surfaces. The curvature of the blades helps in capturing the maximum energy from the orbiting particles. . For the phase position of 0^o-90^o, the maximum momentum is transferred from the water to the rotor because the orbits are elliptical in the present case. It is interesting to note that the pressure does not reduce anywhere during the energy transfer from the orbiting particles to the rotor (the rotor blades do not work like hydrofoils where the pressure drops on the suction side) thus eliminating any risk of cavitation, although the wave induced pressure does provide some acceleration to the particles in their orbital motion.

Figure 6 shows the velocity vectors around the 90º rotor at a frequency of 0.9 Hz and submergence of *1.06d* for the case when the particles are rising and moving forward with the crest (θ = 0º - 90º). It can be seen that the rotor is not receiving much energy from the orbiting particles. When the particles are falling and moving backwards with the trough (phase position θ = 180º -270º), there is still no rotation. It is observed that the particles are undergoing orbital motion around the rotor. The same amount of energy is transferred to the rotors from the orbiting particles. The 90^o rotor does not have effective rotation because the blades are unable to capture the kinetic energy from the orbiting particles. The flat blades do not experience the similar force as the rotors with curved blades, as they are not as streamlined as the curved blades to enable maximum momentum transfer.

In the next round of experiments, four identical rotors, R1, R2, R3 and R4 were placed next to each other (at the same submergence) and the effect of spacing between the rotors on their rpm was studied. Figure 7 shows the variation of the non-dimensional rotor rpm, N_n, averaged over the frequency range investigated and nearly equal to those at the frequency of 0.9 Hz, with the centre-to-centre distance between the rotors (c) which is normalized with the diameter of the rotor. The rotational speeds of the rotors were normalized with those of the first rotor when the spacing between the rotors (c) is minimum (*1.03d*). The submergence of the rotors was *1.21d*. The rotational speeds were found to decrease as the rotor spacing increased, except for the rotor R1 for which the speed increased by nearly 10% from the minimum spacing to the maximum. The direction of rotation of all the rotors is clock-wise when the wave motion is in x-direction. It is interesting to

observe that N_n of a particular rotor is always greater than its preceding rotor (except for *c/d = 2* when the speeds of all the rotors are equal), which indicates that the preceding rotor directs the flow towards the blades of the next rotor located on top at that instant. Moreover, the rotors in the back experience lesser drag due to being in the wake of the front ones, which results in an increase in their rotational speeds. At the same time, it is also clear that vortex shedding from the front rotor does not have any role in the rotation of the rotors. In the present work, the power output of the rotors could not be measured with reasonable accuracy because, due to the light weight of the rotors, they were not responding well to a practical load that can be measured accurately. Nevertheless, it is expected that at low damping coefficients, the behaviour of the rotor will not be significantly different from the undamped case (Coola et al., 1994; Eriksson et al., 2005; Child et al., 2007). However, the power output is expected to peak at a particular frequency in the case of harmonic waves. However, in the case of ocean waves, the peak may not be pronounced at a particular frequency due to the broad distribution of frequencies (Eriksson et al., 2005).

The results of the PIV measurements for the case when the submergence of the rotors is *z/d* = -1.21 and the spacing is *c/d* = 1.03 are shown in Fig. 8. The phase position is $\theta = 0^o$-90^o for this case with the crest approaching the measurement area. It can be seen that the rotors are properly aligned to receive the energy of the orbiting particles and their direction of rotation is matching the orbital motion. It is also observed that when the wave crest is approaching the top of the rotors, there is a strong velocity component in the x-direction which imparts considerable momentum to the blades that receive that flow. Another interesting observation that can be made from the PIV results is that the flow exiting a front rotor did not exert a retarding force on the back rotor, as not much of the flow could penetrate the small spacing between the rotors. In these experiments, it was possible to capture the flow around only three rotors due to the size of the measurement grid that was achievable with the available instrumentation. When the spacing between the rotors was increased to *c/d* = 2.0, the flow around only two rotors could be captured with the PIV system. However, these experiments provided enough information on the flow around the rotors for different spacings.

Figure 9 shows the velocity vectors around two rotors for the submergence of *z/d* = -1.21 and the spacing of *c/d* = 2.0. For this spacing, it was found that the momentum transfer from the orbiting

particles to the rotor is less compared to the case when the rotors are close to each other. One of the reasons for this is the higher drag force experienced by rotors at the back as the flow in the wake of the upstream rotor regains its momentum. For this particular spacing, the velocity vectors could only be captured around two rotors because of the larger distance between them and the fixed size of the measurement grid.

The final round of experiments was conducted with two arrays of three rotors of diameters 86 mm and 66 mm with the larger diameter rotors forming the upper array (R1, R2 and R3) and the smaller diameter rotors forming the lower array (R4, R5 and R6) as shown in Fig. 10. In these experiments, initially the spacing between the upper array of large rotors was varied, keeping their submergence constant, to study the effect of spacing on the rpm of the rotors R1, R2 and R3. It was found that the rpm of these rotors is higher for smaller spacings and the trend was similar to Fig. 7.

Hence, the only parameter that was varied in these experiments was the submergence of the lower array of rotors of diameter 66 mm. The centre-to-centre distance of the upper and lower arrays of rotors (s) was varied and its effect on the rpm of the rotors was studied.

Figure 11 shows the effect of submergence of the 66 mm diameter rotors below the 86 mm diameter rotors. It can be seen that when the distance between the arrays is less, the rpm of the upper rotors as well as the rpm of the lower rotors are higher. The flow through the reduced gap is expected to accelerate for smaller spacing, thus transferring higher momentum to the rotors. As the gap between the upper rotors and lower rotors increases, the rpm of all the rotors reduce. This is due to two reasons: for increased spacing, some of the energy of the rotating particles is not getting utilized in the gap, and 2) the lower array will receive lesser energy from the orbital motion as the energy available reduces with increasing depth (Faizal et al., 2010; Ahmed et al. 2010). It is interesting to note that for both the upper and lower arrays, the rotational speeds of the rotors at the rear are always higher than those of the rotors at the front. Similar observations were reported earlier by Ahmed et al. [2010]. However, for the lower array, the increase in rpm from R4 to R5 and R6 was found to be less compared the rotors in the upper array. This was due to the larger spacing between the lower array rotors.

In the actual case of the ocean waves, multiple arrays of Savonius rotors can be employed with the rotors at different depths matching the orbital size at that depth. The initial work will require finding the diameters of the orbits at different depths. With the help of multiple arrays of rotors, a wave energy farm can be built. Such a wave energy farm can be used to generate the required amount of power without causing much harm to the environment.

4. Conclusions

The orbital motion present in water waves is studied in a wave channel with intermediate depth waves; this orbital motion is utilized to drive Savonius rotors with different blade curvatures. PIV is used to observe the particle behavior around the rotors. Non-dimensioned values of rotor rpm, N_n, are presented for different cases. It is found that the rotor with 70^o blade curvature has the highest rotational speeds. The rotor with 90^o blade curvature did not have effective rotation. Effect of spacing between four rotors was also studied and it is found that the rotors at the rear have higher rpm and that maximum energy capture takes place for minimum spacing between the rotors. In the last study, two arrays of 3 rotors were tested in the wave channel and it was found that when the gap between the arrays is less, the rotational speeds are higher. This concept can be extended to multiple arrays of rotors and large amount of power can be generated with such a wave energy farm.

References

Ahmed, M.R., Faizal, M., Prasad, K., Lee, Y.H., Kim, C.G., Cho, Y.J., 2010. Exploiting the orbital motion of water particles for energy extraction from the waves. Journal of Mechanical Science and Technology 24, 943-949.

Chang, H.K., Liou, J.C., Su, M.Y., 2007. Particle trajectory and mass transport of finite amplitude waves in water of uniform depth. European J Mechanics B Fluids 26, 385–403.

Child, B.F.M., Venugopal, V., 2007. Interaction of waves with an array of floating wave energy devices, Paper No. 1059, Proceedings of the 7th European Wave and Tidal Energy Conference, Protugal.

Coola, P.M., Ravindran, M., Narayana, P.A.A., 1994. Model studies of oscillating water column wave-energy device, ASCE J. Energy Engineering, 14-26.

Dalrymple, RA, Dean, RG., 1991. Water wave mechanics for engineers and scientists, World Scientific Publishing Co. Pte. Ltd., Singapore.

Eriksson, M. Isberg, J. Leijon, M., 2005. Hydrodynamic modelling of a direct drive wave energy converter, International Journal of Engineering Science, 1377-1387.

Faizal, M, Ahmed, MR, Lee, YH., 2010. On utilizing the orbital motion in water waves to drive a Savonius rotor. Renewable Energy 35, 164-169.

Faizal, M, Ahmed, MR, Kim, CG, Lee, YH. 2011. Experimental investigation of water wave characteristics in a wave channel. International Journal of Fluid Mechanics Research 38, 167-178.

Falnes, J., 2007. A review of wave-energy extraction. Marine Structures 20, 185–201.

Hindasageri, V., Ramesh, H., Kattimani, SC. 2011. Performance of Savonius rotors for utilizing the orbital motion of ocean waves in shallow waters. Journal of Sustainable Energy and Environment, 117-119.

Hindasageri, V., Ramesh, H., Gaurav, A. 2012. Effect of variation of wave height and ocean depth on the performance of Savonius rotors utilizing the orbital motion of ocean waves in shallow water. Journal of Sustainable Energy and Environment, 53-57.

Holthuijsen, L.H., 2007. Waves in oceanic and coastal waters. Cambridge Univ. Press, United Kingdom.

Janssen, P., 2004. The interaction of ocean waves and wind. 1st ed. Cambridge Univ. Press, United Kingdom.

Jobb, G. An ocean wave energy converter. Available online at, http://www.treefinder.de/Ideas/WaveConverter.pdf (Accessed 2008).

McCormick, M.E., 2007. Ocean wave energy conversion, 1st ed. Dover Publications, New York.

Mehaute, B.L., 1976. An introduction to hydrodynamics and water waves. 1st ed. Springer, New York.

Merriam, M.F., 1978. Wind, waves, and tides. Annual Review of Energy, 29–56.

Pedlosky, J., 2003. Waves in the ocean and atmosphere: introduction to wave dynamics, 1st ed. Springer, Berlin Heidelberg.

Pelc, R., Fujita R.M., 2002. Renewable energy from the ocean. Marine Policy, 471–479.

Pickard, G.L., Pond, S., 2000. Introductory dynamical oceanography, 3rd ed. Butterworth-Heinemann, Oxford.

Raffel, M., Willert, C., Kompenhans, J., 1998. Particle image velocimetry – a practical guide, 1st ed.

Springer, Berlin Heidelberg.

Rahman, M., 1994. Water waves – relating modern theory to advanced engineering practice, Oxford Univ. Press, New York.

Rea, M., 2008. Wave tank and wavemaker design. In: Cruz Joa˜o, editor. Ocean wave energy – current status and future perspectives, Springer, Berlin Heidelberg.

Reupke, P., Probert, S.D., 1991. Slatted-blade Savonius wind-rotors. Applied Energy, 65–75.

Stagonas, D., Muller, G., 2007. Wave field mapping with particle image velocimetry. J Ocean Eng, 1781–1785.

Twidell, J., Weir, A.D., 2006. Renewable energy resources, 2nd ed. Taylor and Francis, New York.

Figure 1
Click here to download Figure: Figure 1.pdf

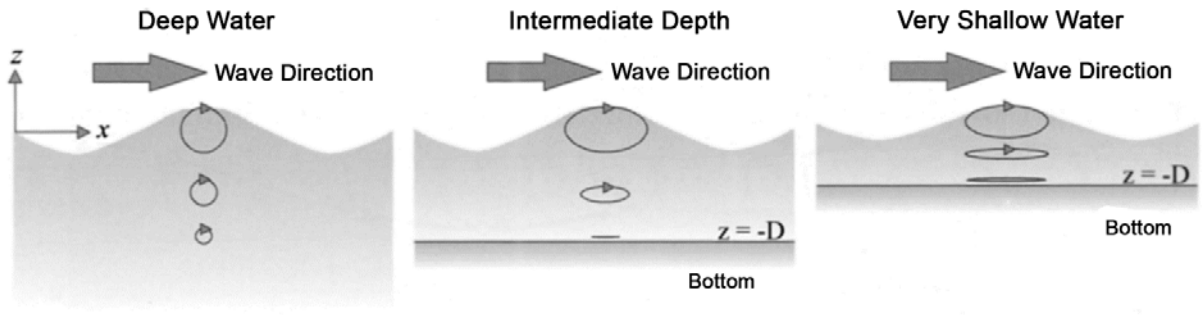

Figure 1. The orbital motion in deep water, intermediate-depth water and shallow water waves (Holthuijsen, 2007).

Figure 2
Click here to download Figure: Figure 2.pdf

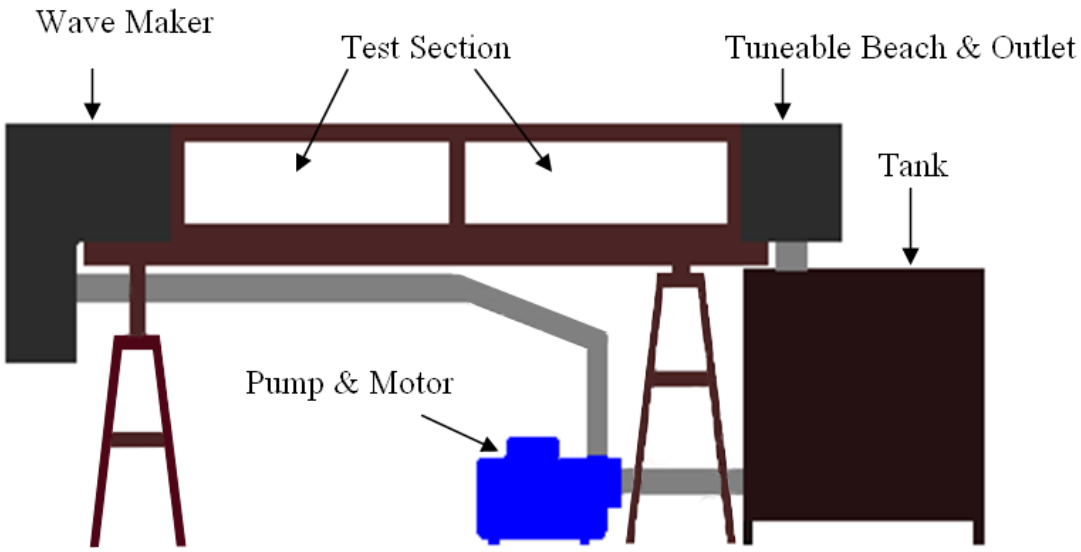

Figure 2. Schematic diagram of the Wave Channel.

Figure 3
Click here to download Figure: Figure 3.pdf

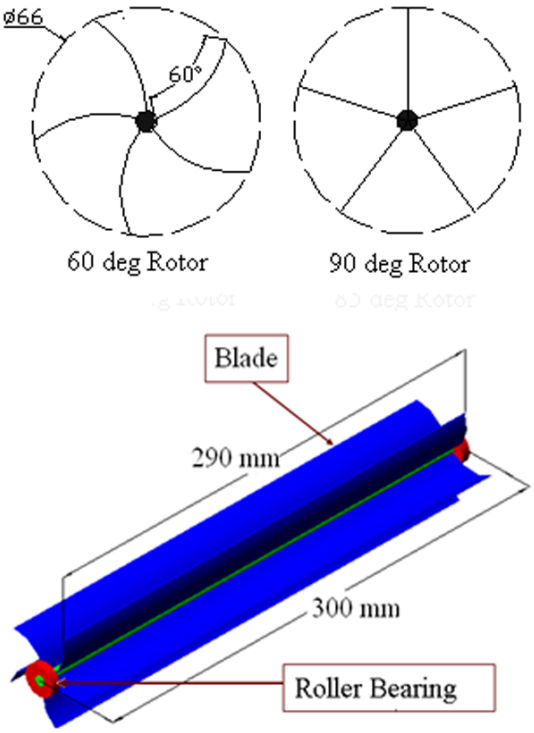

Figure 3. Geometric details of the rotors. Only 60° and 90° rotors are shown here.

Figure 4
Click here to download Figure: Figure 4.pdf

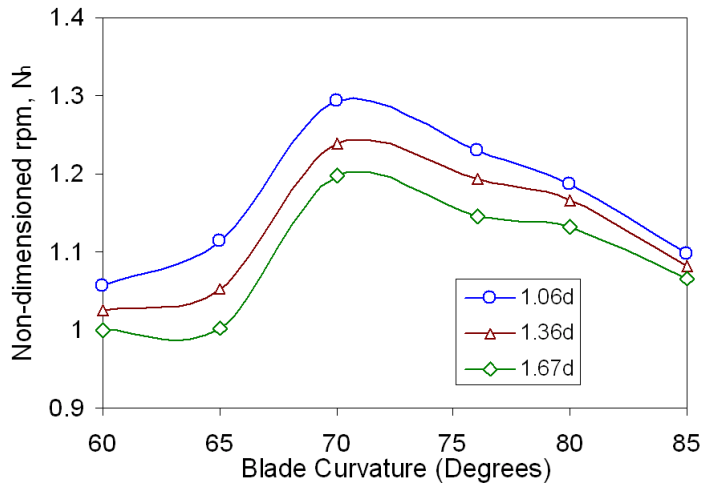

Figure 4. Variation of rotor rpm with different blade curvatures at three submergence levels of the rotor.

Figure 5
Click here to download Figure: Figure 5.pdf

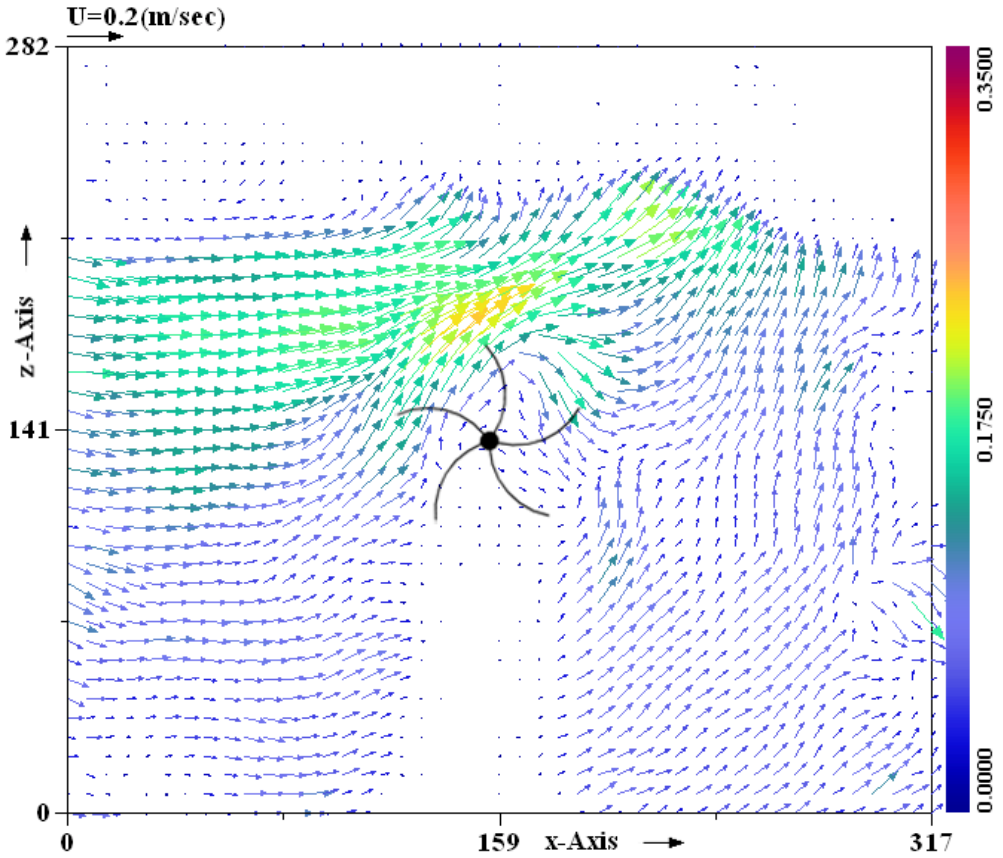

Figure 5. Velocity vectors around the 76° rotor for the phase position of θ = 0° – 90° at *f* = 0.9 Hz and *z/d* = -1.06.

Figure 6
Click here to download Figure: Figure 6.pdf

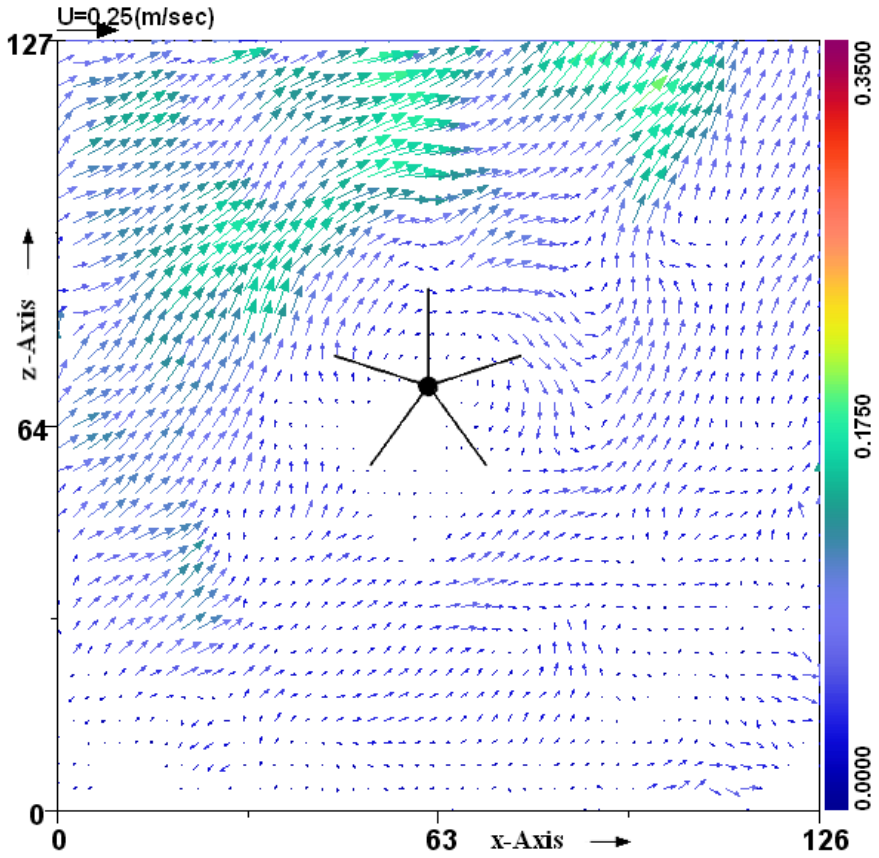

Figure 6. Velocity vectors around the 90° rotor for the phase position of θ = 0° – 90° at *f* = 0.9 Hz and *z/d* = -1.06.

Figure 7
Click here to download Figure: Figure 7.pdf

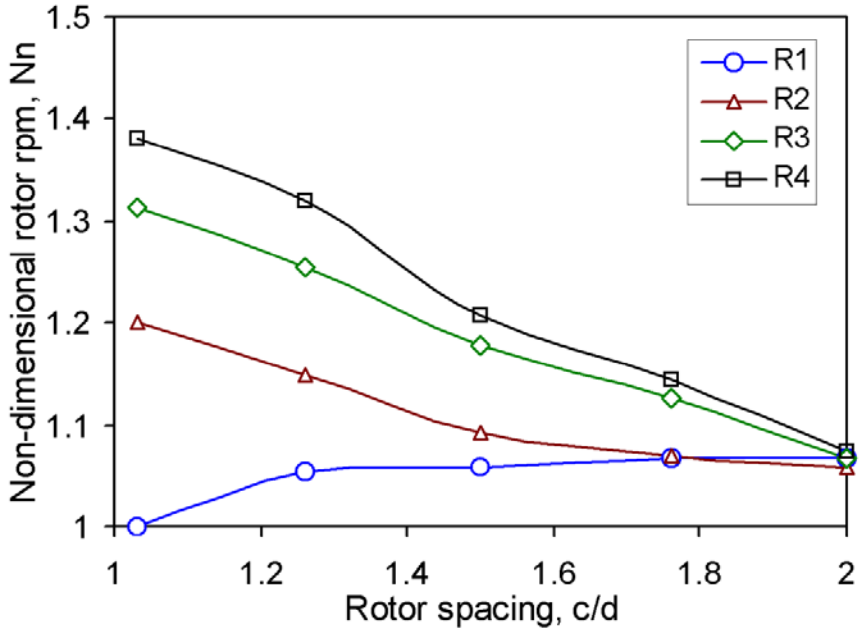

Figure 7. Variation of the rotor's rpm with the centre-to-centre distance between the rotors for z/d = -1.21 (Ahmed et al., 2010).

Figure 8
Click here to download Figure: Figure 8.pdf

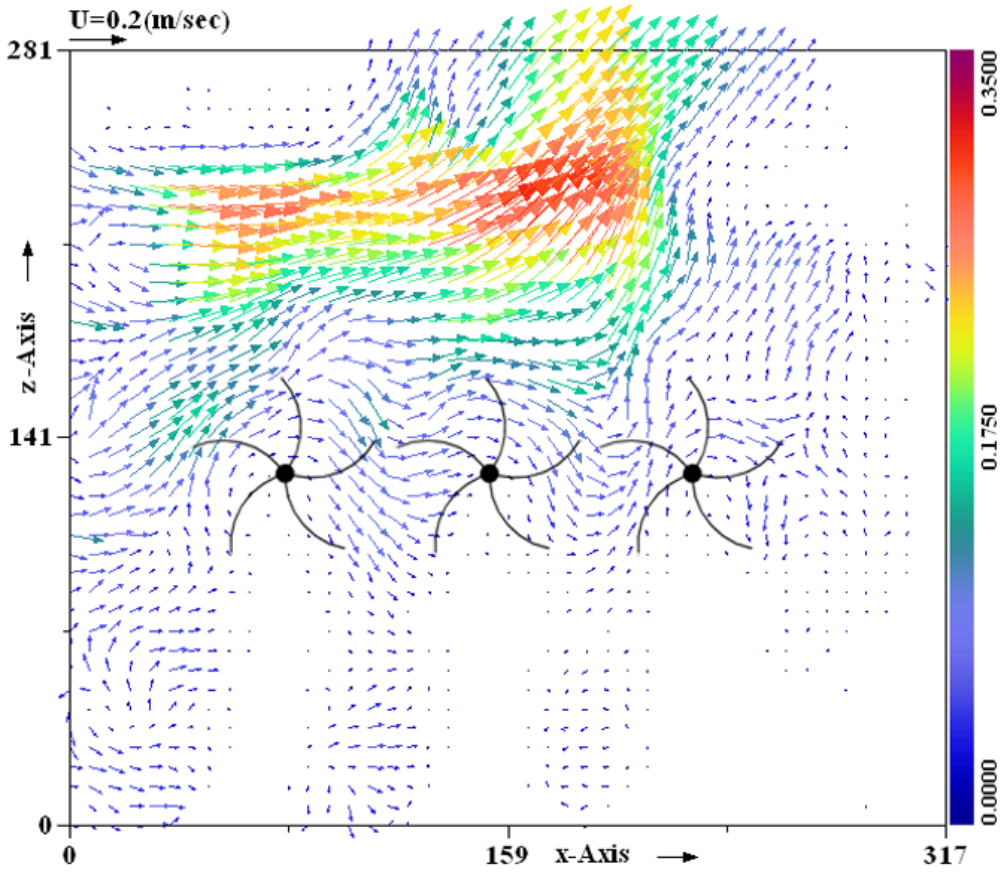

Figure 8. Velocity vectors showing the interaction of the particles with the first three rotors for the phase position of θ = 0^o – 90^o at a frequency of 0.9 Hz for the rotor spacing of c/d = 1.03 and submergence of z/d = -1.21.

Figure 9
Click here to download Figure: Figure 9.pdf

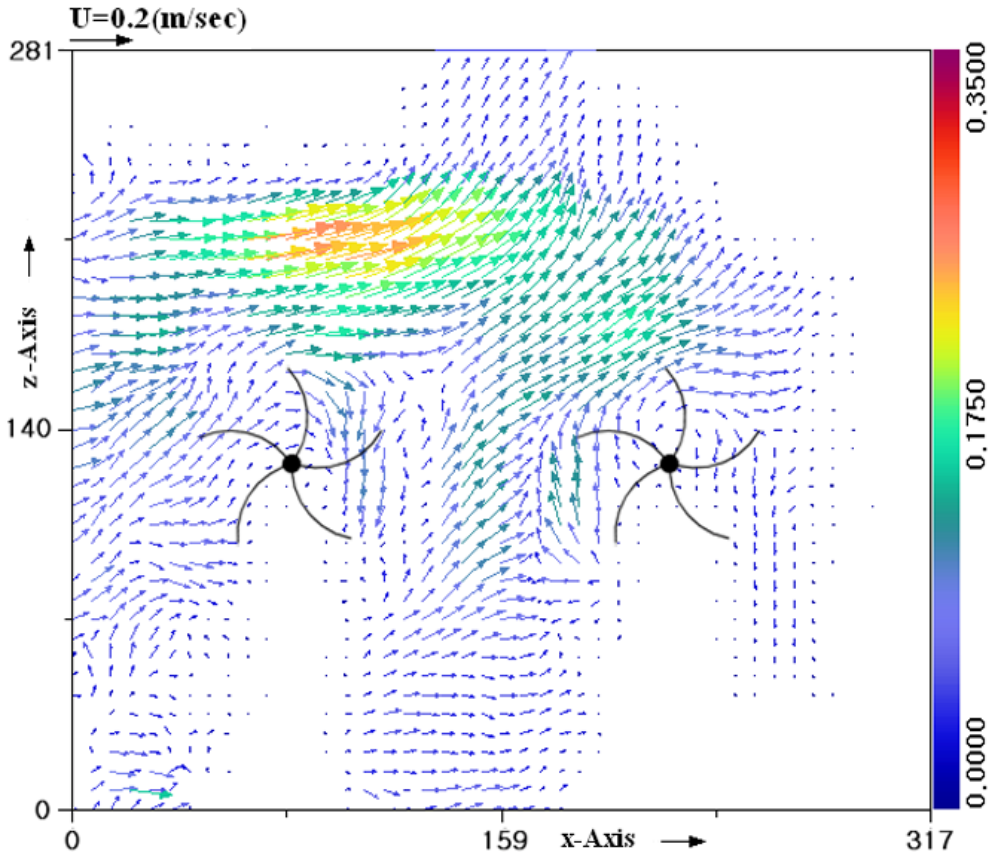

Figure 9. Velocity vectors showing the interaction of the particles with the first two rotors for the phase position of θ = 0^{o} – 90^{o} at a frequency of 0.9 Hz for the rotor spacing of *c/d* = 2.0 and submergence of *z/d* = -1.21.

Figure 10
Click here to download Figure: Figure 10.pdf

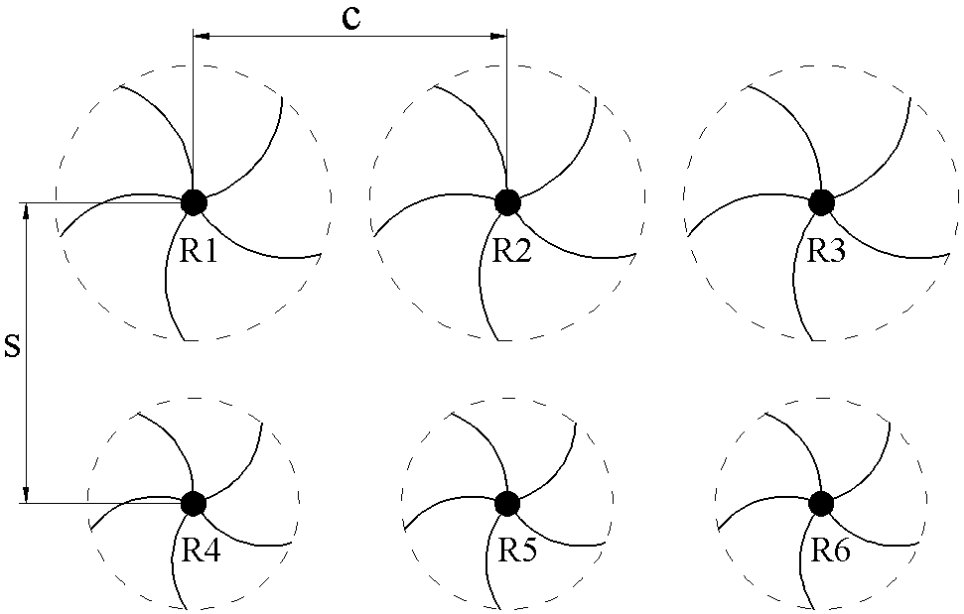

Figure 10. Two arrays of three rotors each with the upper array (R1, R2 and R3) at a submergence of z/d = -1.1 and the lower array (R4, R5 and R6) at a distance s below the upper one.

Figure 11
Click here to download Figure: Figure 11.pdf

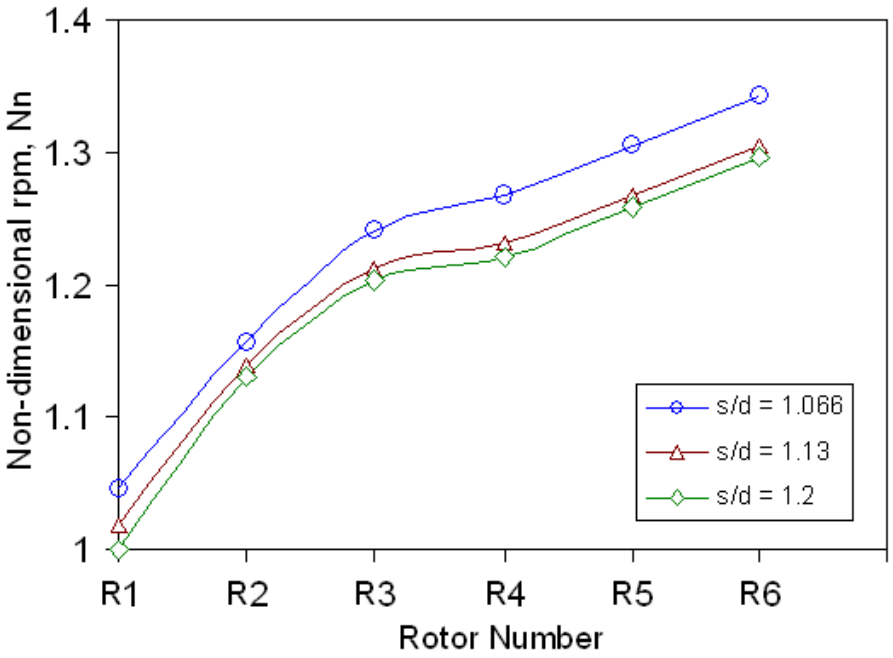

Figure 11. Effect of submergence of the lower array of rotors below the upper array on the rpm of the rotors.

Table 1

Table 1: Experimental variables and settings

Set Number	Mean Water Depth, D (mm)	Wave frequency, *f* (Hz)	Rotor Diameter, *d* (mm)	Rotor Submergence (mm)	Rotor Spacing, c (mm)
1	260	0.9	66	70, 80, 90, 100, 110	Not Applicable
2	260, 290	0.8, 0.9, 1.0	66, 86	70, 80, 90	68, 83, 99, 116, 132
3	260, 290	0.9	66, 86	80, 90, 95	68, 88